# PCCP

Physical Chemistry Chemical Physics

## Accepted Manuscript

This article can be cited before page numbers have been issued, to do this please use: P. Zhang, W. Lee and S. Ye, *Phys. Chem. Chem. Phys.*, 2024, DOI: 10.1039/D4CP02915A.

Volume 19
Number 1
7 January 2017
Pages 1-896

PCCP

Physical Chemistry Chemical Physics

rsc.li/pccp

ISSN 1463-9076

ROYAL SOCIETY OF CHEMISTRY

PAPER
H.-P. Loock *et al.*
Determination of the thermal, oxidative and photochemical degradation rates of scintillator liquid by fluorescence EEM spectroscopy

ARTICLE

View Article Online
DOI: 10.1039/D4CP02915A

# Insights into Dioxygen Binding on Metal Centers: An ab initio Multireference Electronic Structure Analysis

Received 00th January 20xx,
Accepted 00th January 20xx

DOI: 10.1039/x0xx00000x

Peng Zhang,[a,b] Way-Zen Lee[c,d] and Shengfa Ye *[a]

Why does binding of dioxygen ($O_2$) to metal centers, the initial step of $O_2$ storage, transportation, and activation, almost inevitably induce metal-to-$O_2$ single-electron transfer and generate superoxo ($O_2^{-\cdot}$) species, instead of genuine $O_2^0$ adducts? To address this question, this study describes highly correlated wavefunction based ab initio calculations using CASSCF/NEVPT2 (CASSCF = complete active space self-consistent field, and NEVPT2 = N-electron valence state second-order perturbation theory) approaches to explore the electronic-structure evolution of $O_2$ binding on Fe(II)(BDPP) ($H_2$BDPP = 2,6-bis((2-(S)-diphenylhydroxylmethyl-1-pyrrolidinyl)methyl)pyridine) and Co(II)(BDPP) to produce $S$ = 3 Fe(III)(BDPP)($O_2^{-\cdot}$) (**1**) and $S = \frac{1}{2}$ Co(III)(BDPP)($O_2^{-\cdot}$) (**2**). CASSCF/NEVPT2 calculations suggest that the $O_2$ binding processes furnishing **1** and **2** feature an avoided crossing resulting from interactions of two diabatic curves, of which one is characterized as Co(II) and Fe(II) centers interacting with a triplet $O_2$ ligand and the other as Co(III) and Fe(III) centers bound to a superoxo ligand. In both cases, the avoided crossing induces a one-electron transfer from the divalent metal center to the incoming $O_2$ ligand and leads to formation of trivalent metal-$O_2^{-\cdot}$ complexes. To facilitate interpretation of complicated multireference wavefunctions, we formulated two-fragment spin eigenfunctions utilizing Clebsch-Gordan coefficients (CGCs) to rationalize computed spin populations on metal centers and $O_2$ ligand and compared it with usual valence bonding (VB) analyses. It turns out that both methods give the same results and are complementary to each other. Finally, the limitation of DFT approaches in describing complex electronic structures involving metal-ligand magnetic coupling is delineated.

## Introduction

Binding of dioxygen ($O_2$) on metal cofactors of metalloproteins initiates a diverse array of physiologically pivotal processes, including $O_2$ storage, transportation, and activation for substrate functionalization.[1-6] Myoglobin, a heme enzyme containing a high spin ferrous center, reacts with $O_2$ yielding a singlet Fe-$O_2^{-\cdot}$ complex,[7-9] while for nonheme enzymes isopenicillin N synthase (IPNS)[10-12] and homoprotocatechuate 2,3-dioxygenase (Fe-HPCD),[13-15] $O_2$ addition results in a quintet Fe-$O_2^{-\cdot}$ adduct that is best described as a high spin ferric center ($S_{\mathrm{Fe}} = \frac{5}{2}$) antiferromagnetically coupled to a superoxo ligand ($O_2^{-\cdot}$) ($S_{O_2^{-\cdot}} = \frac{1}{2}$) yielding an overall $S_{\mathrm{t}}$ = 2 ground state. To mimic enzymatic $O_2$ binding, numerous model complexes have been synthesized and characterized.[16-18] The reactions of $O_2$ with a range of ferrous complexes, such as Fe(II)(BNPA$^{Me2}$S)(Br) (BNPA$^{Me2}$SH = bis((6-(neopentylamino)pyridinyl)methyl)amino)-2-methylpropane-2-thiol),[19] (L$^{Ad}$H)Fe (L$^{Ad}$H = tris(phosphinimine) ligand),[20] Fe($S_2$$^{Me2}$$N_3$(Pr,Pr))[21] and Fe(ttppc) (ttppc$^{3-}$ = 5, 10, 15-tris((2,4,6-triphenyl)phenyl)corrolate)[22] all yield similar quintet Fe-$O_2$ adducts. In contrast to examples discussed above, treatment of $O_2$ with a high spin Fe(II) precursor ($S_{\mathrm{Fe}}$ = 2), Fe(II)(BDPP) ($H_2$BDPP = 2,6-bis((2-(S)-diphenylhydroxylmethyl-1-pyrrolidinyl)methyl)pyridine) at 193 K generates $S_{\mathrm{t}}$ = 3, instead of $S_{\mathrm{t}}$ = 2, Fe(III)(BDPP)($O_2^{-\cdot}$) (**1**) attained by ferromagnetic coupling of a high spin Fe(III) center ($S_{\mathrm{Fe}} = \frac{5}{2}$) and a $O_2^{-\cdot}$ ligand ($S_{O_2^{-\cdot}} = \frac{1}{2}$).[23] While the corresponding reaction with high spin Co(II)(BDPP)[24] ($S_{\mathrm{Co}} = \frac{3}{2}$) at 193 K furnishes a doublet Co(III)-$O_2^{-\cdot}$ species, Co(III)(BDPP)($O_2^{-\cdot}$) (**2**), which has been characterized as consisting of a low spin Co(III) center ($S_{\mathrm{Co}}$ = 0) interacting with a $O_2^{-\cdot}$ ligand ($S_{O_2^{-\cdot}} = \frac{1}{2}$).[25] Furthermore, the same product was also found for $O_2$ addition to Co-HPCD,[26] the Co derivative of Fe-HPCD, and a plethora of high spin or low spin Co(II) complexes, including Co-TPP (TPP$^{2-}$ = tetraphenylporphyrinate),[27] Co($Me_3$TACN)($S_2SiMe_2$) ($Me_3$TACN = 1,4,7-trimethyl-1,4,7-triazacyclononane),[28] Co(Tp$^{Me2}$)($^{tBu2}$APH) (Tp$^{Me2}$ = hydrotris(3,5-dimethylpyrazolyl)borate,[29] $^{tBu2}$APH = 2-amino-4,6-di-tert-butylphenol), Co(salen)[30] and Co(Por) (Por = porphyrin).[31] Over-decade intensive investigations revealed that $O_2$ association on divalent nonheme metal centers almost inevitably entails a metal-to-$O_2$ electron transfer and thus produces a trivalent metal-$O_2^{-\cdot}$ complex.[32,33] To the best of our knowledge, there is only one exception; $O_2$ binding on a variant of Fe-HPCD labelled as Y257F-HPCA, was proposed to form a Fe(II)-$O_2$ intermediate, instead of Fe(III)-$O_2^{-\cdot}$.[34-38] An intriguing question thus arises about whether it is viable to engender such authenticated $O_2$ adducts from $O_2$ association on metal centers.

In parallel to intensive experimental research, a great deal of computational studies have been devoted to probing electronic structures of $O_2$ adducts and evaluating electronic-structure evolution over the course of $O_2$ binding processes.[39-47] In this regard, density functional theory (DFT) calculations usually cannot yield satisfactory results, especially for those systems featuring antiferromagnetic coupling of two fragments. In principle, such a complicated electronic structure cannot be appropriately described by a single Slater determinant. Consequently, broken symmetry formalism has to be invoked, because of the inherent single determinant restriction of DFT approaches.[48]

The Kohn-Sham solution thus obtained is no longer the eigenfunction of $\hat{S}^2$; consequently, the resulting spin density is not correct, and the following spin population analysis are physically unjustified. To obtain more accurate electronic structures, one has to resort to highly correlated wavefunction based multireference approaches.[39,40,41,45,47] To date, these methods have been successfully applied to the $O_2$ adducts of heme systems, but hardly to nonheme ones.[33] To the best of our knowledge, only one ab initio study has been reported thus far where potential energy curves of varying spin states were computed for $O_2$ association on a heme center.[49] This work does not focus on elucidation of electronic-structure changes occurring during this process but on the quintet-to-singlet spin crossover; hence, it does not provide sufficient information to address the aforementioned question.

In the present work, we describe a detailed multireference analysis of the electronic-structure evolution as $O_2$ steadily approaches the Fe(II) and Co(II) centers in Fe(II)(BDPP) and Co(II)(BDPP) affording **1** and **2**, respectively.

---

[a] State Key Laboratory of Catalysis, Dalian Institute of Chemical Physics, Chinese Academy of Sciences, Dalian 116023, China.
[b] University of Chinese Academy of Sciences, Beijing 100049, China.
[c] Department of Chemistry, National Taiwan Normal University, Taipei 11677, Taiwan.
[d] Department of Medicinal and Applied Chemistry, Kaohsiung Medical University, Kaohsiung 807, Taiwan

View Article Online
DOI: 10.1039/D4CP02915A

Specifically, highly correlated wavefunction based complete active space self-consistent field (CASSCF)[50]/*N*-electron valence state second-order perturbation theory (NEVPT2)[51,52] computations were carried out on a series of geometric structures on the reaction trajectory generated by DFT computations. To interpret complicated multireference wavefunctions of $O_2$ adducts, we constructed two-fragment spin eigenfunctions using Clebsch-Gordan coefficients (CGCs)[53] to rationalize computed spin populations. CASSCF/NEVPT2 calculations suggest that the $O_2$ binding processes furnishing **1** and **2** feature an avoided crossing of two diabatic curves that represent Fe(II)/Co(II)-$O_2^0$ and Fe(III)/Co(III)-$O_2^{-\cdot}$ limiting valence structures each. Their interaction induces a spontaneous single-electron transfer from the divalent metal center to the incoming $O_2$ ligand, thereby leading to formation of trivalent metal-$O_2^{-\cdot}$ complexes as the final product for the $O_2$ binding processes.

## Computation setup

To obtain the reaction trajectory for formation of complexes **1** and **2**, the M-$O_2$ distance was steadily varied from 1.75 to 4.50 Å in an *S* = 3 and an *S* = $\frac{1}{2}$ state, respectively, in relaxed surface scans conducted by using the B3LYP functional[54,55] in conjunction with the def2-TZVP basis set[56-58] for N, O, Fe, and Co, and the def2-SVP basis set[59,60] for other atoms (C and H atoms). Moreover, RIJCOSX approximations[61] were employed in combination with the def2/J auxiliary basis set[62,63] to speed up DFT computations. To take solvation effects into consideration, the CPCM model[64] with THF as the solvent was applied, and D3BJ corrections[65,66] were used to account for dispersion corrections. Frequency analysis on a given optimized geometry structure was performed to computed its zero point energy (ZPE) and thermal correction. To compute reliable electronic structures, CASSCF calculations with def2-TZVP basis set for all atoms were carried out at each geometric structure of the reaction trajectory. As verified below, the appropriate active space of complexes **1** and **2** is chosen to distribute 12 and 13 electrons, respectively, into 9 orbitals including five metal 3d based orbitals (five spherical 3d orbitals are used here), two $O_2$ π bonding ($\pi_{ip}$ and $\pi_{op}$) and the corresponding π* antibonding ($\pi_{ip}^*$ and $\pi_{op}^*$) orbitals. For complex **1**, CASSCF calculations average a triplet, a quintet, and a septet state, and for complex **2**, a doublet, a quartet, and a sextet state were considered. Based on the converged state-average CASSCF wavefunction, complete active space configuration interaction (CASCI) calculations were employed to calculate spin density and spin populations of a specific spin state. On top of CASSCF wavefunctions, NEVPT2 computations were undertaken to obtain more precise electronic energies. To accelerate ab initio computations, RIJK approximations[67] in conjunction with the def2/JK auxiliary basis set[68] were used. Thus, the final potential energy surface was constructed by the electronic energy derived from CASSCF/NEVPT2 calculations combined with the ZPE contribution and thermal corrections. All computations were performed with the ORCA-5.0.3 program package.[69]

## Results and discussion

### Choice of active spaces

Unlike DFT, CASSCF is not a black box method, because as the first step to initiate CASSCF calculations users should prudently select a proper active space, which requires users to have some preliminary understanding of the electronic structure of the system under investigation. To ensure that the chosen active space is sufficient to provide reliable electronic structures, further calculations are often necessary with enlarged and/or truncated active spaces. Critically, CASSCF computations with suitable active spaces not only yield precise electronic structures, but also result in fast convergence. Usually, because d and f orbitals of transition metal compounds are nearly degenerate which leads to strong multiconfiguration character, these orbitals should be included in the active space. Equally important is that, to properly describe a metal-ligand covalent bond, the active space ought to contain its bonding and antibonding molecular orbital (MO). Otherwise, the CASSCF computation with an unbalanced active space would result in incorrect electronic structure. Both criteria were used to choose a suitable active space for our CASSCF calculations.

In the present case, in addition to 5 metal 3d based orbitals, two π bonding ($\pi_{ip}$ and $\pi_{op}$) and two π* antibonding ($\pi_{ip}^*$ and $\pi_{op}^*$) orbitals of the $O_2$ ligand should be included in the active space. It should be pointed out that, as elaborated below, this active space can properly describe the metal-$O_2$ covalent bonding built from the metal 3d and $O_2$ π* fragment orbitals of appropriate symmetry. Therefore, the active spaces of complexes **1** and **2** were chosen to distribute 12 and 13 electrons, respectively, in 9 orbitals. Depicted in **Fig. 1** is the active space of complex **2** obtained by the CASSCF(13,9) computation at the Co-$O_2$ bond length of 2.50 Å. An analogous active space was employed for complex **1**.

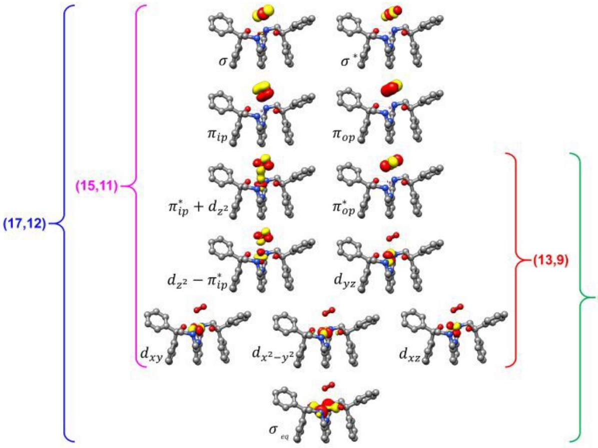

**Fig. 1**. Different choices of active spaces (m,n) (m electrons in n orbitals) for complex **2** at the Co-$O_2$ bond length of 2.50 Å. For clarity, hydrogen atoms are omitted for clarity.

To test the appropriateness of the selected active space, we took complex **2** at the Co-$O_2$ bond length of 2.50 Å as an example and performed a series of CASSCF computations with different active spaces. First, we added $BDPP^{2-}$ O and N 2p donor based $\sigma_{eq}$ into the active space that is the $\sigma$ bonding counterpart with respect to $d_{x^2-y^2}$. Accordingly, two more electrons ought to be added into the active space, thereby resulting in an active space of CAS(15,10). Second, we constructed an active space of CAS(15,11) by including $O_2$ σ and σ$^*$ orbitals into the active space to take the entire 2p shells of the $O_2$ moiety into consideration and. Third, an even larger active space of CAS(17,12) was built up to consider all the aforementioned effects. As summarized in **Table 1**, the occupation numbers of $\sigma_{eq}$ are invariably 2 for all key electron configurations of each spin state derived from CASSCF(15,10) calculations. Similarly, those of $O_2$ σ and σ$^*$ are constants of 2 and 0, respectively, for all important electron configurations predicted by CASSCF(15,11) computations. The same holds true for CASSCF(17,12) results. As such, for a given spin state all CASSCF computations give qualitatively the same electronic structures as evidenced by almost identical percentage of each dominant electron configuration and hence spin populations on the Co center and the $O_2$ moiety. Moreover, we have also performed CASSCF calculations with these three distinct active spaces on complex **2** at a longer (4.50 Å) and a shorter (1.91 Å) Co-$O_2$ bond length, and again the calculations produced analogous results, see **Fig. S1** and **S2**. In addition, we have also carried out CASSCF(13,9) calculations with different basis sets, such as def2-SV, def2-SVP, def2-TZVP and def2-TZVPP, and the same electronic structures were obtained as listed in **Tables S1** – **S3**. In summary, the active space of

View Article Online
DOI: 10.1039/D4CP02915A

CAS(13,9) and the def2-TZVP basis set are sufficient to yield reliable electronic structures and bonding features for complex **2** at varying Co-$O_2$ bond distances. Likewise, CASSCF(12,9) with the def2-TZVP basis set ought to produce satisfactory results for the $O_2$ association process affording complex **1** as well.

**Table 1.** Spin populations on Co center and $O_2$ moiety and electron configurations for each spin state from CASSCF calculations with different choices of active orbitals for complex **2** at the Co-$O_2$ bond length of 2.50 Å.

| | configuration | | | spin populations | | |
|---|---|---|---|---|---|---|
| | sextet | quartet | doublet | sextet | quartet | doublet |
| CASSCF(13,9)<br>$d_{xz}d_{yz}d_{xy}d_{x^2-y^2}(d_{z^2}-\pi_{ip}^{*})\pi_{op}\pi_{ip}\pi_{op}^{*}(\pi_{ip}^{*}+d_{z^2})$ | 87% 221112211 | 42% 221112211<br>14% 221102212<br>10% 221122210<br>9% 221012212<br>6% 221212210 | 21% 221112211<br>21% 221102212<br>14% 221122210<br>13% 221012212<br>9% 221212210 | Co<br>2.83 (2.88)<br>$O_2$<br>1.98 (2.00) | Co<br>2.08 (2.11)<br>$O_2$<br>0.79 (0.80) | Co<br>1.56 (1.59)<br>$O_2$<br>-0.65 (-0.66) |
| CASSCF(15,10)<br>$\sigma_{eq}d_{xz}d_{yz}d_{xy}d_{x^2-y^2}(d_{z^2}-\pi_{ip}^{*})\pi_{op}\pi_{ip}\pi_{op}^{*}(\pi_{ip}^{*}+d_{z^2})$ | 87% 2221112211 | 43% 2221112211<br>15% 2221102212<br>10% 2221122210<br>8% 2221012212<br>5% 2221212210 | 22% 2221112211<br>22% 2221102212<br>15% 2221122210<br>11% 2221012212<br>8% 2221212210 | Co<br>2.83 (2.88)<br>$O_2$<br>1.98 (1.99) | Co<br>2.08 (2.11)<br>$O_2$<br>0.79 (0.80) | Co<br>1.56 (1.59)<br>$O_2$<br>-0.65 (-0.66) |
| CASSCF(15,11)<br>$d_{xz}d_{yz}d_{xy}d_{x^2-y^2}(d_{z^2}-\pi_{ip}^{*})\pi_{op}\pi_{ip}\pi_{op}^{*}(\pi_{ip}^{*}+d_{z^2})\sigma\sigma^{*}$ | 87% 22111221120 | 46% 22111221120<br>19% 22110221220<br>13% 22112221020<br>3% 22101221220<br>2% 22121221020 | 20% 22111221120<br>30% 22110221220<br>21% 22112221020<br>5% 22101221220<br>4% 22121221020 | Co<br>2.83 (2.88)<br>$O_2$<br>1.98 (1.99) | Co<br>2.07 (2.11)<br>$O_2$<br>0.80 (0.80) | Co<br>1.56 (1.59)<br>$O_2$<br>-0.65 (-0.66) |
| CASSCF(17,11)<br>$\sigma_{eq}d_{xz}d_{yz}d_{xy}d_{x^2-y^2}(d_{z^2}-\pi_{ip}^{*})\pi_{op}\pi_{ip}\pi_{op}^{*}(\pi_{ip}^{*}+d_{z^2})\sigma\sigma^{*}$ | 87% 222111221120 | 47% 222111221120<br>19% 222110221220<br>13% 222112221020<br>3% 222101221220<br>2% 222121221020 | 21% 222111221120<br>31% 222110221220<br>21% 222112221020<br>5% 222101221220<br>3% 222121221020 | Co<br>2.83 (2.88)<br>$O_2$<br>1.98 (1.99) | Co<br>2.07 (2.11)<br>$O_2$<br>0.80 (0.80) | Co<br>1.56 (1.59)<br>$O_2$<br>-0.65 (-0.66) |

### $O_2$ binding on Fe(II)(BDPP) affording complex 1

Depicted in **Fig. 2** is the $S_{\mathrm{t}}$ = 3 potential energy surface of the $O_2$ bonding to the high spin Fe(II)(BDPP) calculated by CASSCF(12,9) /NEVPT2 computations. As expect, starting point $^{7}$**A** with a Fe-$O_2$ bond length of 4.00 Å is best interpreted as a high spin Fe(II) ion ($S_{\mathrm{Fe}}$ = 2) ferromagnetically coupled with a triplet $O_2$ ligand ($S_{O_2}$ = 1) yielding an overall septet state. Consistent with this assignment, ab initio calculations suggested that this state is distinguished by a leading electron configuration of $d_{xz}{}^{2}d_{yz}{}^{1}d_{xy}{}^{1}d_{x^2-y^2}{}^{1}d_{z^2}{}^{1}\pi_{ip}{}^{2}\pi_{op}{}^{2}\pi_{ip}^{*}{}^{1}$ $\pi_{op}^{*}{}^{1}$ (95%). As shown in **Fig. 2**, the computed spin density and spin populations (Löwdin analysis, 3.86 for Fe and 2.00 for $O_2$; Mulliken analysis, 3.91 for Fe and 2.00 for $O_2$) further corroborate this electronic-structure formulation. Of note, because spin populations estimated by Löwdin and Mulliken analyses are essentially the same, in the following we only discuss the former but list the latter in **Fig. 2**. As the $O_2$ ligand steadily approaches the Fe center, the energy of this valence structure invariably rises as shown by the corresponding diabatic potential curve (magenta line). During this process, the nature of the Fe-$O_2$ bonding remains essentially the same as indicated by the unchanged spin populations on the Fe(II) center and the $O_2$ ligand, for instance, complex $^{7}$**B**. However, starting from the Fe-$O_2$ distance of 2.30 Å, CASSCF(12,9) calculations could converge to another solution as exemplified by complex $^{7}$**1**. It features a sole electron configuration of $d_{xz}{}^{1}$ $(d_{yz}+\pi_{op}^{*})^{1}d_{xy}{}^{1}d_{x^2-y^2}{}^{1}(d_{z^2}-\pi_{ip}^{*})^{1}\pi_{ip}{}^{2}\pi_{op}{}^{2}(\pi_{ip}^{*}+d_{z^2})^{2}(\pi_{op}^{*}-d_{yz})^{1}$ (100%) and is best described as a high spin Fe(III) center ($S_{\mathrm{Fe}} = \frac{5}{2}$) ferromagnetically coupled with a superoxo ligand ($S_{O_2^{\cdot-}} = \frac{1}{2}$) as suggested by the computed spin density and spin populations (4.74 for Fe and 1.03 for $O_2$). Its energy first descends for the Fe-$O_2$ distance ranging from 2.30 Å to 2.06 Å and then ascends as the Fe-$O_2$ distance further decreases; thus, its diabatic potential curve (crimson curve) displays a local minimal ($^{7}$**1**) at the Fe-$O_2$ distance of ~2.00 Å.

The interaction of the aforementioned two diabatic potential curves results in an avoided crossing near the Fe-$O_2$ bond length of 2.30 Å and a barrier of 13.6 kcal/mol. Moreover, the entire process is moderately endothermic with a driving force of 8.0 kcal/mol. Given the unfavorable entropy contribution for combination reactions, this value should be somewhat overestimated by our computations, because experimentally $^{7}$**1** is stable at low temperatures (< 193 K) but releases $O_2$ affording Fe(II)(BDPP) upon raising temperature. The overestimation of the binding barrier can be ascribed to the fact that the active space employed does not suffice to capture escalating electron correlations at the transition state where two diabatic surfaces strongly interact. Nevertheless, the entire process can be interpreted as shifting one β electron from the Fe $d_{xz}$ orbital to the $O_2$ $\pi_{ip}^{*}$ orbital, thus leading to the formation of $^{7}$**1**. As indicated by the septet potential surface, because in the avoided crossing region an energetically favorable electron transfer from the Fe(II) center to the $O_2$ ligand takes place, which allows the system to ultimately convert into $^{7}$**1**, it is unlikely to trap the proposed Fe(II)-$O_2$ complex during this $O_2$ binding process. In line with this prediction, UV-vis measurements at 193 K showed that no intervening intermediate could be detected en route to $^{7}$**1**.[23]

Experimentally, the $O_2$ adducts of IPNS[10-12] and Fe-HPCD[13-15] have been spectroscopically identified to be quintet Fe(III)-superoxo species. However, our CASSCF(12,9)/NEVPT2 computations could not allow to determine the exact ground state of complex **1**, because the estimated septet-quintet energy gap of 2.4 kcal/mol falls within the range of uncertainty for ab initio calculations. Thus, we also investigated the reaction of Fe(II)(BDPP) with $O_2$ in an $S_{\mathrm{t}}$ = 2 state. As shown in **Fig. 2**, the quintet potential energy surface computed for the $O_2$ binding process is essentially parallel to the septet one in the sense that there exists an analogous avoided crossing around the Fe-$O_2$ distance of 2.30 Å derived from interactions of two diabatic potential curves, yielding a barrier of 11.3 kcal/mol. Furthermore, the quintet reaction also entails a comparable driving force of 5.6 kcal/mol. As elaborated below, the diabatic potential curve starting with complex $^{5}$**A** describes the energy variation of an $S_{\mathrm{t}}$ = 2 state attained by magnetic coupling of a high spin Fe(II) center ($S_{\mathrm{Fe}}$ = 2) and a triplet $O_2$ ligand ($S_{O_2}$ = 1) as a function of the Fe-$O_2$ distance; the other one represents that consisting of a high spin Fe(III) center ($S_{\mathrm{Fe}} = \frac{5}{2}$) that is antiferromagnetically coupled with a doublet superoxo ligand ($S_{O_2^{\cdot-}} = \frac{1}{2}$).

View Article Online
DOI: 10.1039/D4CP02915A

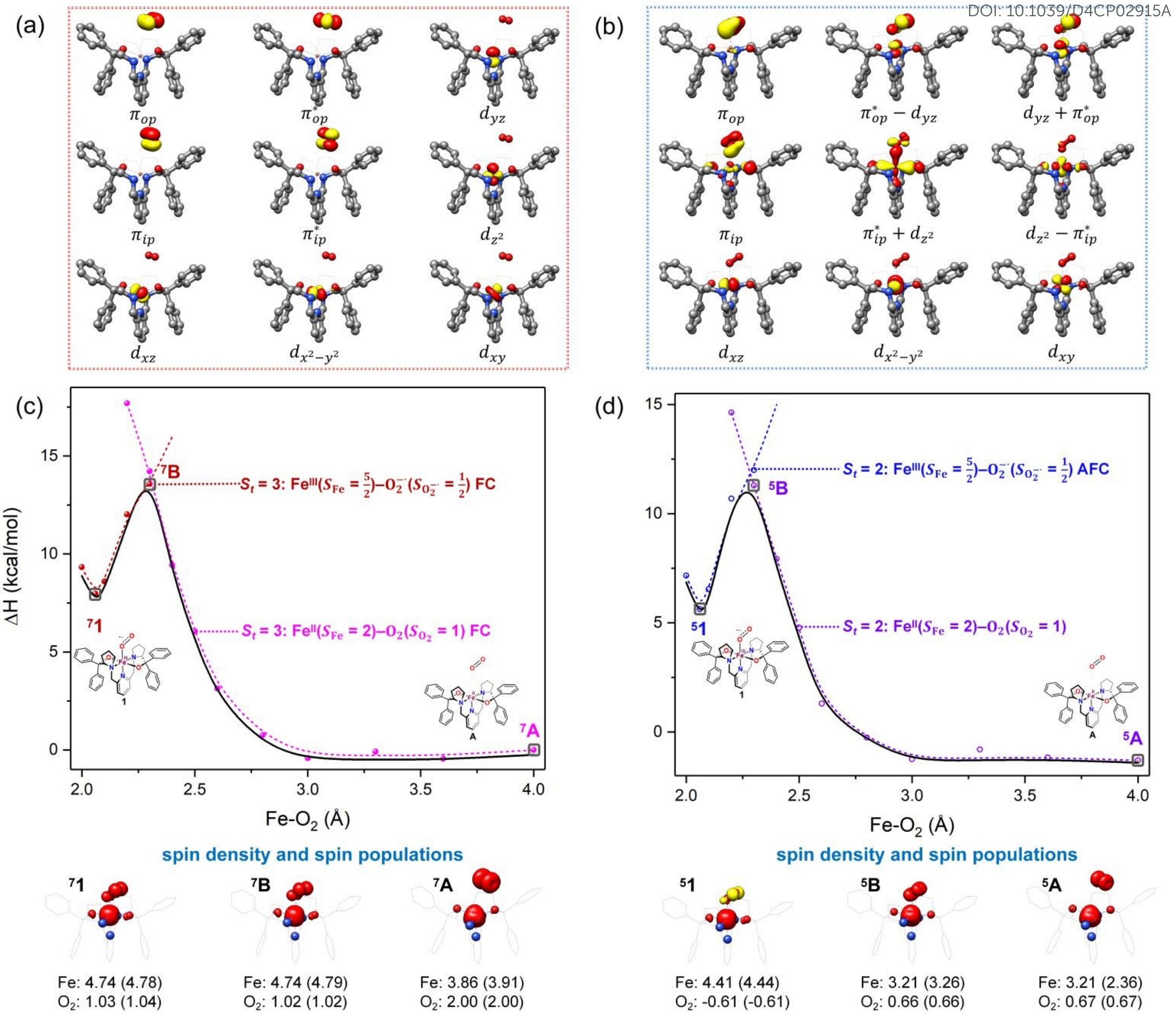

**Fig. 2** Active spaces of complexes **A** (a) and **1** (b); septet potential energy surface for the reaction of Fe(II)(BDPP) with $O_2$ as a function of the Fe−$O_2$ bond distance obtained by CASSCF(12,9)/NEVPT2 computations; dot lines denote diabatic potential curves (magenta line denotes an $S_t$ = 3 Fe$^{II}$-$O_2$ complex consisting of as an $S_{Fe}$ = 2 Fe$^{II}$ center ferromagnetically coupled (FC) with an $S_{O_2}$ = 1 $O_2$ ligand; crimson line denotes an $S_t$ = 3 Fe$^{III}$-$O_2^{-\cdot}$ complex consisting of an $S_{Fe} = \frac{5}{2}$ Fe$^{III}$ center ferromagnetically coupled (FC) with an $S_{O_2^{-\cdot}} = \frac{1}{2}\, O_2^{-\cdot}$ ligand) and black line denotes adiabatic curve for reaction on *S* = 3 potential surface; spin density and Löwdin and Mulliken (in parentheses) spin populations on the Fe center and the $O_2$ unit calculated for complexes $^7$**A** (Fe(II)(BDPP) + $O_2$), $^7$**B**, and $^7$**1** on the reaction trajectory are shown at the bottom, yellow and red denote negative and positive spin density, respectively, and local spin populations were also listed in the Supporting Information (c); quintet potential energy surface for the reaction of Fe(II)(BDPP) with $O_2$ as a function of the Fe−$O_2$ bond distance obtained by CASSCF(12,9)/NEVPT2 computations; dot lines denote diabatic potential curves (violet line denotes a quintet state Fe$^{II}$-$O_2$ complex, interpreted as an $S_{Fe}$ = 2 Fe$^{II}$ compound magnetically coupled with an $S_{O_2}$ = 1 $O_2$ ligand; blue line denotes a quintet state Fe$^{III}$-$O_2^{-\cdot}$ complex, interpreted as an $S_{Fe} = \frac{5}{2}$ Fe$^{III}$ center antiferromagnetically coupled (AFC) with an $S_{O_2^{-\cdot}}$ $O_2^{-\cdot}$ ligand) and black line denotes adiabatic curve for reaction on *S* = 3 potential surface; spin density and Löwdin and Mulliken (in parentheses) spin populations on Fe center and $O_2$ unit calculated for complexes $^5$**A** (Fe(II)(BDPP) + $O_2$), $^5$B, and $^5$**1** on the reaction trajectory are shown at the bottom, yellow and red denote negative and positive spin density, respectively, and local spin populations were also listed in the Supporting Information (d);ligand atoms are omitted for clarity.

Ab initio calculations reveal that complex $^5$**A** is isoenergetic to $^7$**A** and, importantly, the leading electron configuration $d_{xz}{}^2 d_{yz}{}^1 d_{xy}{}^1 d_{x^2-y^2}{}^1 d_{z^2}{}^1 \pi_{ip}{}^2 \pi_{op}{}^2 \pi^*_{ip}{}^1 \pi^*_{op}{}^1$ (94%) of the former species is also the same as that of the latter. This can be traced back the large Fe-$O_2$ separation that prevents any nonnegligible metal-ligand interactions from occurring. Following this line of reasoning, $^5$**A** should contain a quintet Fe(II) center ($S_{Fe}$ = 2) that is exchange coupled to a triplet $O_2$ ligand ($S_{O_2}$ = 1). However, the spin populations calculated for the Fe center (3.21) and the $O_2$ ligand (0.67) are far from those one would expected for non-interacting $S_{Fe}$ = 2 Fe(II) and $S_{O_2}$ = 1 $O_2$

fragments. To solve this problem, the vector coupling model was invoked to construct the spin eigenfunction with a well-defined total spin $S$ of the resulting state derived from the magnetic coupling of a high spin Fe(II) center and a triplet O$_2$ ligand using CGCs. In the present case, the former entity can be characterized by spin eigenfunction $|S_1,M_1\rangle = |2,M_1\rangle$ ($M_1 = \pm 2, \pm 1, 0$), and the latter by $|S_2,M_2\rangle = |1,M_2\rangle$ ($M_2 = \pm 1, 0$). The quintet state originating from the magnetic coupling of these two fragments should be distinguished by spin eigenfunction $|S,M\rangle = |2,M\rangle$ ($M = \pm 2,, \pm 1, 0$), and its standard component reads $|2,2\rangle = \sqrt{\frac{2}{3}}|2,2|1,0\rangle - \sqrt{\frac{1}{3}}|2,1|1,1\rangle$, where for brevity the functions on the right hand of the equal sign are abbreviated as $|S_1,M_1|S_2,M_2\rangle$. This spin eigenfunction features $\hat{S}_z$ expectation values (the spin projection along the z axis) of $\frac{5}{3}$ and $\frac{1}{3}$ for the Fe(II) center and the O$_2$ unit, respectively. Indeed, both values are in line with the computed spin populations (3.21 for Fe and 0.67 for O$_2$), because, ideally spin populations are twice the $\hat{S}_z$ expectation values, thus affirming the proposed electronic-structure assignment.

Regarding the O$_2$ binding process furnishing $^5$**1**, as the Fe-O$_2$ distance decreases from 4.00 Å to 2.30 Å (violet curve), the wavefunction steadily acquires multireference character having three dominant electron configurations of ${d_{xz}}^2{d_{yz}}^1{d_{xy}}^1{d_{x^2-y^2}}^1(d_{z^2}-\pi^*_{ip})^1{\pi_{ip}}^2{\pi_{op}}^2(\pi^*_{ip}+d_{z^2})^1{\pi^*_{op}}^1$ , ${d_{xz}}^2{d_{yz}}^1{d_{xy}}^1{d_{x^2-y^2}}^1(d_{z^2}-\pi^*_{ip})^0{\pi_{ip}}^2{\pi_{op}}^2(\pi^*_{ip}+d_{z^2})^2{\pi^*_{op}}^1$, and ${d_{xz}}^2{d_{yz}}^1{d_{xy}}^1{d_{x^2-y^2}}^1(d_{z^2}-\pi^*_{ip})^2{\pi_{ip}}^2{\pi_{op}}^2(\pi^*_{ip}+d_{z^2})^0{\pi^*_{op}}^1$. These three electron configurations differ in their varying occupation number in $\pi^*_{ip}+d_{z^2}$ and $d_{z^2}-\pi^*_{ip}$ orbitals, both of which, in fact, describe the covalent interaction between Fe(II) center and O$_2$ ligand (**Fig. 1**). During this process, the weight of the first one plummets from 94% to 57%, while those of the last two rise from 0% to 21% and 12%, respectively, suggesting the progressively strengthened covalent Fe-O$_2$ interaction. However, the spin density and spin populations computed for $^5$**B** are analogous to those for $^5$**A**. This finding demonstrates that the electronic structure of $^5$**B** is nearly the same as that of $^5$**A**, indicative of weak covalent Fe-O$_2$ interaction of $^5$**B**. As the Fe-O$_2$ bond length further declines, one electron is shifted from the Fe(II) center to the O$_2$ ligand near the avoided crossing region accompanied by a rapid adjustment of the electronic structure of the nascent Fe(III) center to afford $^5$**1** in the end.

CASSCF(12,9) calculations reveal that the quintet state of complex $^5$**1** features strong multireference character and consists of three key electron configurations of ${d_{xz}}^1(d_{yz}+\pi^*_{op})^1{d_{xy}}^1{d_{x^2-y^2}}^1(d_{z^2}-\pi^*_{ip})^1{\pi_{ip}}^2{\pi_{op}}^2(\pi^*_{ip}+d_{z^2})^2(\pi^*_{op}-d_{yz})^1$ (38%), ${d_{xz}}^1(d_{yz}+\pi^*_{op})^0{d_{xy}}^1{d_{x^2-y^2}}^1(d_{z^2}-\pi^*_{ip})^1{\pi_{ip}}^2{\pi_{op}}^2(\pi^*_{ip}+d_{z^2})^2(\pi^*_{op}-d_{yz})^2$ (36%), and ${d_{xz}}^1(d_{yz}+\pi^*_{op})^2{d_{xy}}^1{d_{x^2-y^2}}^1(d_{z^2}-\pi^*_{ip})^1{\pi_{ip}}^2{\pi_{op}}^2(\pi^*_{ip}+d_{z^2})^2(\pi^*_{op}-d_{yz})^0$ (25%). Apparently, this wavefunction is too complex to extract any chemically sensible bonding information from its predominant electron configurations. Specifically, the first one could be interpreted as a high spin Fe(III) center ($S_{\mathrm{Fe}} = \frac{5}{2}$) antiferromagnetically coupled to a doublet superoxo ligand ($S_{\mathrm{O}_2^{-\cdot}} = \frac{1}{2}$), the second one as a quintet Fe(IV) center ($S_{\mathrm{Fe}} = 2$) bound to a singlet peroxo ligand ($S_{\mathrm{O}_2^{2-}} = 0$), and the last one as a high spin Fe(II) center ($S_{\mathrm{Fe}} = 2$) coordinated by a singlet O$_2$ ligand ($S_{\mathrm{O}_2} = 0$). However, as demonstrated in **Fig. 2**, the spin density calculated for complex $^5$**1** exhibits a spherical shape for the Fe center, reminiscent of the high spin Fe(III) center ($S_{\mathrm{Fe}} = \frac{5}{2}$) in complexes $^7$**B** and $^7$**1**, but different from the high spin Fe(II) center ($S_{\mathrm{Fe}} = 2$) in complexes $^7$**A** and $^5$**A**. Moreover, the spin density reveals substantial negative spin primarily populating O$_2$ $\pi^*_{op}$ orbital, thereby signaling that the O$_2$ ligand is best described as a doublet superoxo ligand ($S_{\mathrm{O}_2^{-\cdot}} = \frac{1}{2}$). Based on these findings, we surmised that complex $^5$**1** is best described as a high spin Fe(III) center ($S_{\mathrm{Fe}} = \frac{5}{2}$) antiferromagnetically coupled with a superoxo ligand ($S_{\mathrm{O}_2^{-\cdot}} = \frac{1}{2}$) affording an overall $S_{\mathrm{t}} = 2$ state. Following the route used to interpret the electronic structure of $^5$**A**, such a bonding situation should be described by $|2,2\rangle = \sqrt{\frac{5}{6}}\left|\frac{5}{2},\frac{5}{2}\middle|\frac{1}{2},-\frac{1}{2}\right\rangle - \sqrt{\frac{1}{6}}\left|\frac{5}{2},\frac{3}{2}\middle|\frac{1}{2},\frac{1}{2}\right\rangle$. This spin eigenfunction furnishes $\hat{S}_z$ expectation values of $\frac{7}{3}$ and $-\frac{1}{3}$ for the Fe center and the O$_2$ ligand, respectively, congruent with the computed spin populations (4.41 for Fe and –0.61 for O$_2$), affirming the bonding interpretation.

View Article Online
DOI: 10.1039/D4CP02915A

Alternatively, to interpret the multireference wavefunction computed for complex $^5$**1**, valence bonding (VB) reading was also employed as exemplified by VB analysis of the electronic structure of the myoglobin O$_2$ adduct reported by Sason and coworkers.[70] As shown in **Fig. 3**, upon localization of $d_{yz}+\pi^*_{op}$ and $\pi^*_{op}-d_{yz}$ , representing bonding and antibonding interactions of $d_{yz}$ and $\pi^*_{op}$, the ground state wavefunction re-expressed in the basis of the localized orbitals ($d_{yz}$ and $\pi^*_{op}$) contains merely one electron configuration of ${d_{xz}}^1{d_{yz}}^1{d_{xy}}^1{d_{x^2-y^2}}^1{d_{z^2}}^1{\pi_{ip}}^2{\pi_{op}}^2{\pi^*_{ip}}^2{\pi^*_{op}}^1$ (99%), whereas the original one in the basis of natural orbitals exhibits strong multireference character having three dominant electron configurations as discussed above. It should be pointed out that both wavefunctions are equivalent, because they are related by a unitary transformation of orbitals in the active space. Moreover, the computed spin density and spin populations reveal that the majority spin is located on the Fe center and the minority one of the opposite sign on the O$_2$ ligand. As such, two electrons, which are spin paired, are located on $d_{yz}$ and $\pi^*_{op}$ MOs, respectively. Both findings therefore approve of the electronic-structure assignment put forward above.

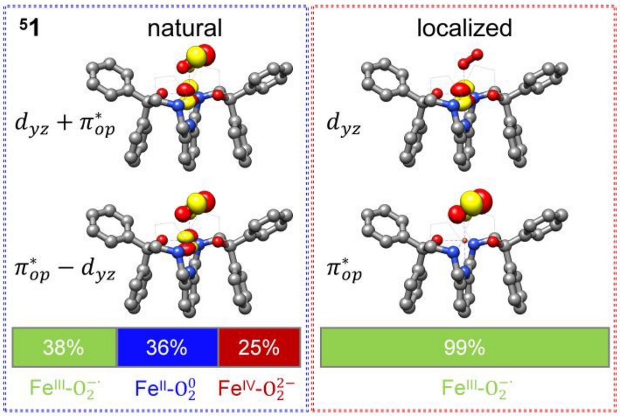

**Fig. 3** $d_{yz}$ and $\pi^*_{op}$ MOs in natural and localized forms with the electron configurations and their weights for $^5$**1** complex; Fe$^{\mathrm{III}}$-$\mathrm{O}_2^{-\cdot}$ denotes the electron configuration of ${d_{xz}}^1(d_{yz}+\pi^*_{op})^1{d_{xy}}^1{d_{x^2-y^2}}^1(d_{z^2}-\pi^*_{ip})^1{\pi_{ip}}^2{\pi_{op}}^2(\pi^*_{ip}+d_{z^2})^2(\pi^*_{op}-d_{yz})^1$, Fe$^{\mathrm{IV}}$-$\mathrm{O}_2^{2-}$ represents the electron configuration of ${d_{xz}}^1(d_{yz}+\pi^*_{op})^0{d_{xy}}^1{d_{x^2-y^2}}^1(d_{z^2}-\pi^*_{ip})^1{\pi_{ip}}^2{\pi_{op}}^2(\pi^*_{ip}+d_{z^2})^2(\pi^*_{op}-d_{yz})^2$, and Fe$^{\mathrm{II}}$-O$_2$ indicates the electron configuration of ${d_{xz}}^1(d_{yz}+\pi^*_{op})^2{d_{xy}}^1{d_{x^2-y^2}}^1(d_{z^2}-\pi^*_{ip})^1{\pi_{ip}}^2{\pi_{op}}^2(\pi^*_{ip}+d_{z^2})^2(\pi^*_{op}-d_{yz})^0$, ligand atoms are omitted for clarity.

Clearly, in the case of complex $^5$**1**, VB analyses is as efficient as constructing two-fragment spin eigenfunction to interpret its multireference wavefunction. However, this approach is not applicable to complex $^5$**A** where the absence of covalent interactions between the Fe center and the O$_2$ ligand renders localization fruitless. It follows that VB analyses cannot be used to characterize multireference wavefunctions without strong electron correlations. In this respect, our simple approach does not have such a limitation.

The reaction of Fe(II)(BDPP) with O$_2$ in an $S_{\mathrm{t}} = 1$ state also features two diabatic potential curves; one denotes a high spin Fe(II) center ($S_{\mathrm{Fe}} = 2$)

antiferromagnetically coupled with a triplet $O_2$ ligand ($S_{O_2}$ = 1), and the other describes an intermediate spin Fe(III) center ($S_{\mathrm{Fe}} = \frac{3}{2}$) antiferromagnetically coupled with a doublet superoxo ligand ($S_{O_2^{\cdot -}} = \frac{1}{2}$). Although the triplet transformation is barrierless, it is highly endothermic by 30.2 kcal/mol. (See Supporting Information for more details) and cannot contribute to the actual reaction. Taken together, $O_2$ association on a high spin ferrous center proceeds either on a septet or on a quintet surface, in line with experimentally findings.[23]

### $O_2$ binding Co(II)(BDPP) affording complex 2

As shown in **Fig. 4**, starting from $^2$**C** at a Co−$O_2$ distance of 4.50 Å, the diabatic potential curve (magenta line) of the doublet state arising from the antiferromagnetic coupling of a high spin Co(II) center ($S_{\mathrm{Co}} = \frac{3}{2}$) and a triplet $O_2$ ligand ($S_{O_2}$ = 1) is constantly uphill as the Co-$O_2$ bond length decreases. Furthermore, starting from the Co-$O_2$ distance of 2.50 Å, we could locate another diabatic potential curve (crimson line) that is best described as a low spin Co(III) ion ($S_{\mathrm{Co}} = 0$) interacting with a doublet superoxide radical ($S_{O_2^{\cdot -}} = \frac{1}{2}$). Its energy first decreases for the Co-$O_2$ distance ranging from 2.50 Å to 1.90 Å and then increases for the even shorter Co-$O_2$ distances; hence, a local minimal ($^2$**2**) is located at the Co-$O_2$ length of ~1.90 Å. Two diabatic potential curves interact in the vicinity of the Co-$O_2$ distance being 2.40 Å and generate an avoided crossing with a barrier of 24.7 kcal/mol for the $O_2$ binding reaction affording complex $^2$**2**. Moreover, the entire process is slightly endothermic by 8.4 kcal/mol. In analogy to the $O_2$ association yielding $^7$**1**, our ab initio computations likely overestimate the barrier and the driving force, because experimentally complex $^2$**2** is persistent at low temperatures (< 193 K) but releases $O_2$ upon elevating temperature.[25]

View Article Online
DOI: 10.1039/D4CP02915A

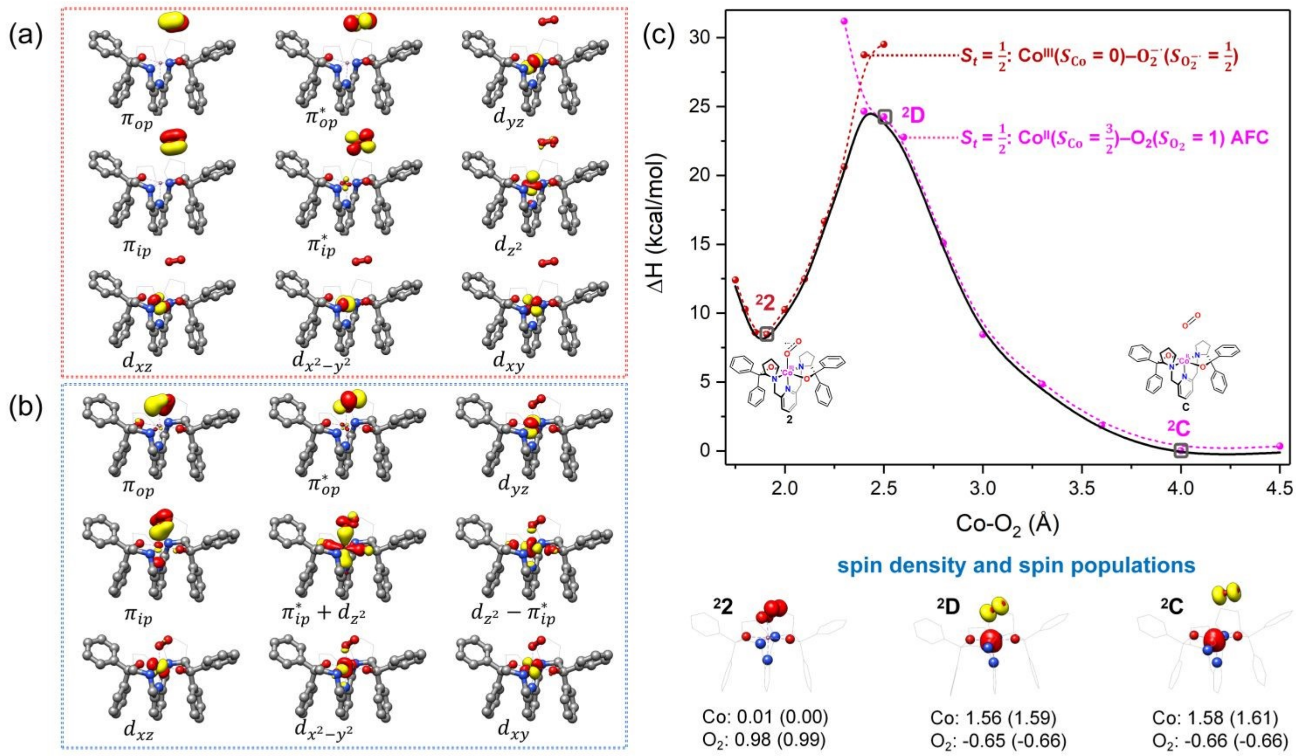

**Fig. 4** Active spaces of complexes **C** (a) and **2** (b); doublet potential energy surface for the reaction of Co(II)(BDPP) with $O_2$ as a function of the Co−$O_2$ bond distance obtained by CASSCF(13,9)/NEVPT2 computations. Dot lines denote diabatic potential curves, namely, magenta line a doublet Co$^{II}$-$O_2$ complex, interpreted as an $S_{\mathrm{Co}} = \frac{3}{2}$ Co$^{II}$ center antiferromagnetically coupled (FC) with a triplet $O_2$ ligand ($S_{O_2}$ = 1); crimson line a doublet Co$^{III}$-$O_2^{\cdot -}$ complex, interpreted as an $S_{\mathrm{Co}}$ = 0 Co$^{III}$ ion interacting with a doublet $O_2^{\cdot -}$ ligand ($S_{O_2^{\cdot -}} = \frac{1}{2}$); black line $S_{\mathrm{t}} = \frac{1}{2}$ adiabatic curve ; spin density and Löwdin and Mulliken (in parentheses) spin populations on the Co center and the $O_2$ ligand calculated for complexes $^2$**C** (Co(II)(BDPP) + $O_2$), $^2$**D** and $^2$**2** on the reaction trajectory are shown at the bottom, yellow and red denote negative and positive spin density, respectively, and local spin populations were also listed in the Supporting Information (c); ligand atoms are omitted for clarity.

CASSCF(13,9) calculations of complex $^2$**C** produces a predominant electron configuration of $d_{xz}{}^2 d_{yz}{}^2 d_{xy}{}^1 d_{x^2-y^2}{}^1 d_{z^2}{}^1 \pi_{ip}{}^2 \pi_{op}{}^2 \pi_{ip}^{*}{}^1 \pi_{op}^{*}{}^1$ accounting for 80% of the wavefunction. As demonstrated in **Fig. 4**, the computed spin density plot exhibits a double-layer donut shape of the $O_2$ ligand, which implies that unpaired electrons equally populate its $\pi_{ip}^*$ and $\pi_{op}^*$ orbitals. Therefore, both findings suggest that complex $^2$**C** is best interpreted as a high spin Co(II) center ($S_{\mathrm{Co}} = \frac{3}{2}$) antiferromagnetically coupled to a triplet $O_2$ ligand ($S_{O_2}$ = 1) yielding an overall $S_{\mathrm{t}} = \frac{1}{2}$ ground state. Again, we constituted two-fragment spin eigenfunctions using CGCs to interpret this wavefunction and it reads $\left|\frac{1}{2},\frac{1}{2}\right\rangle = \frac{1}{\sqrt{2}}\left|\frac{3}{2},\frac{3}{2}\right|1,-1\right\rangle - \frac{1}{\sqrt{3}}\left|\frac{3}{2},\frac{1}{2}\right|1,0\right\rangle + \frac{1}{\sqrt{6}}\left|\frac{3}{2},-\frac{1}{2}\right|1,1\right\rangle$. This spin eigenfunction gives $\hat{S}_z$ expectation values of $\frac{5}{6}$ and $-\frac{1}{3}$ for the Co(II) center and the $O_2$ ligand, respectively. Indeed, both values are in line with the computed spin populations which confirms the proposed electronic-structure assignment.

On the other hand, ab initio calculations suggest that complex $^2$**2** features a leading configuration of $d_{xz}{}^2 d_{yz}{}^2 d_{xy}{}^2 d_{x^2-y^2}{}^0 (d_{z^2} - \pi_{ip}^*)^0 \pi_{ip}{}^2 \pi_{op}{}^2 (\pi_{ip}^* + d_{z^2})^2 \pi_{op}^{*}{}^1$ (95%). Clearly, its electronic structure is best described as a low spin Co(III) center ($S_{\mathrm{Co}}$ = 0) magnetically coupled with a doublet superoxo ligand ($S_{O_2^{\cdot-}}$ = $\frac{1}{2}$), congruent with the computed spin density and spin populations of 0.01 for the Co center and of 0.98 for the $O_2$ moiety as demonstrated in **Fig. 4**.

Regarding the $O_2$ binding process furnishing $^2$**2**, as the Co-$O_2$ distance decreases from 4.50 Å to 2.30 Å (magenta curve), the wavefunction steadily acquires multireference character with three dominant electron configurations of ${d_{xz}}^2{d_{yz}}^2{d_{xy}}^1{d_{x^2-y^2}}^1(d_{z^2}-\pi_{ip}^*)^1{\pi_{ip}}^2{\pi_{op}}^2(\pi_{ip}^*+d_{z^2})^1{\pi_{op}^*}^1$, ${d_{xz}}^2{d_{yz}}^2{d_{xy}}^1{d_{x^2-y^2}}^1(d_{z^2}-\pi_{ip}^*)^0{\pi_{ip}}^2{\pi_{op}}^2(\pi_{ip}^*+d_{z^2})^2{\pi_{op}^*}^1$, and ${d_{xz}}^2{d_{yz}}^2{d_{xy}}^1{d_{x^2-y^2}}^1(d_{z^2}-\pi_{ip}^*)^2{\pi_{ip}}^2{\pi_{op}}^2(\pi_{ip}^*+d_{z^2})^0{\pi_{op}^*}^1$. These three electron configurations differ in their varying occupation number in $\pi_{ip}^*+d_{z^2}$ and $d_{z^2}-\pi_{ip}^*$ orbitals that describe the covalent interaction between Co(II) center and $O_2$ ligand as depicted in **Fig. 1**. During this process, the weights of the last two terms rise from 0% to 34% and 17%, respectively, which comes at the price of the percentage of the first one that lowers from 80% to 22%, signaling the increased Co-$O_2$ bonding strength. However, the electronic structure of $^2$**D** is similar to that of $^2$**C** as evidenced by the comparable spin density and spin populations computed for both species, which suggests that the Co-$O_2$ covalent interaction is rather weak. As the Co-$O_2$ distance further declines, an one-electron transfer from the Co(II) center to the $O_2$ ligand occurs around the avoided crossing region concurrent with a rapid adjustment of the electronic structure of the Co(III) center furnishing complex $^2$**2**.

The doublet potential energy surface of the $O_2$ association process yielding $^2$**2** is also constructed by two diabatic potential curves; one represents the reactant complex containing a high spin Co(II) center ($S_{\mathrm{Co}}$ = $\frac{3}{2}$) antiferromagnetically coupled to a triplet $O_2$ ligand ($S_{O_2}$ = 1) yielding an overall $S_{\mathrm{t}}$ = $\frac{1}{2}$ ground state, and the other describes the product complex consisting of as a low spin Co(III) ion ($S_{\mathrm{Co}}$ = $0$) interacting with a doublet superoxide radical ($S_{O_2^{\cdot-}}$ = $\frac{1}{2}$). For the reaction of Co(II)(BDPP) with $O_2$, the emergence of the avoided crossing region suggests that no intermediate other than $^2$**2** can be observed and that the Co(II)-$O_2$ adduct does not exist, consistent with experimental findings.[25]

For $O_2$ binding on Fe(II)(BDPP) and Co(II)(BDPP), our ab initio calculations show that the former process entails a lower barrier of 13.6 kcal/mol to $^7$**1** than the latter (24.7 kcal/mol) to $^2$**2**. This theoretical prediction is congruent with the experimental observation that generation of $^7$**1** is much faster than that of $^2$**2**.[23,25] Furthermore, both transformations feature an avoided crossing that realizes one-electron transfer from a divalent metal center to $O_2$ and furnishes a trivalent metal center and a superoxo ligand as the final product; consequently, the divalent-$O_2$ adduct cannot be formed.

As elaborated in the section of Introduction, except one case, reactions of $O_2$ with a wide variety of Fe(II) and Co(II) precursors reported thus far all generate Fe(III) or Co(III) superoxo products, which intimates that the avoided crossing found for the $O_2$ addition processes on Fe(II)(BDPP) and Co(II)(BDPP) occurs in those transformations as well. In fact, association of $O_2$ to related Mn(II)(BDPP) complex also produces a Mn(III)-$O_2^{\cdot-}$ complex, instead of Mn(II)-$O_2$.[32] Likewise, treatment of a series of Cu(I) species including [Cu($NH_2$-TMPA)]$^+$ (TMPA = tris-methyl pyridine amine)[71], [Cu($TMG_3$tren)]$^+$ ($TMG_3$tren = tris(tetramethylguanidino)tren)[72] and [Cu($Ar_3$-TMPA)]$^+$ (Ar = tpb, dpb and dtbpb)[73] with $O_2$ invariably afford Cu(II)-$O_2^{\cdot-}$, whereas the authenticated $O_2$ adduct, Cu(I)-$O_2$, has yet to be disclosed. More reactions of $O_2$ and metal complexes affording superoxo adducts were summarized in the review articles.[74-78] However, the reaction of $O_2$ with Y257F-HPCA was proposed to furnish Fe(II)-$O_2$ rather than Fe(III)-$O_2^{\cdot-}$. This proposition was solely based on $^{57}$Fe Mössbauer spectroscopic measurements that give an unambiguous assignment of the Fe oxidation state, but the detailed information about the exact valence state of the $O_2$ ligand remains lacking. Further thorough experimental research is required to verify the advocated electronic-structure assignment, and disprove and/or substantiate our theoretical prediction.

### Comments on DFT Computations

View Article Online
DOI: 10.1039/D4CP02915A

For a given state distinguished by a total spin of $S$, its spin projection along the z axis of $M_{\mathrm{s}}$ features 2$S$+1 values (-$S$, -S+1, ⋯, $S$-1, $S$) and constitutes 2$S$+1 microstate labelled as $|S,M_{\mathrm{s}}\rangle$. Among them, only $|S,S\rangle$ and $|S,-S\rangle$ could be represented by a single Slater determinant and are the eigenfunction of $\hat{S}^2$ and $\hat{S}_z$, whereas others have to be constructed as a linear combination of a series of Slater determinants, all having the eigenvalue of $\hat{S}_z$ of $M_{\mathrm{s}}$, in order to be the eigenfunctions of $\hat{S}^2$. Therefore, single-Slater-determinant approaches such as DFT could only deal with $|S,S\rangle$ and $|S,-S\rangle$. Both are equivalent except for the eigenvalue of $\hat{S}_z$; hence, typically merely $|S,S\rangle$ called standard component is computed. For example, complex $^2$**2** in **Fig. 5**, where the spin populations of Co and $O_2$ are calculated to be –0.02 and 1.00 along with $\langle\hat{S}^2\rangle$ = 0.76 is congruent with the anticipated spin eigenfunction of $\left|\frac{1}{2},\frac{1}{2}\right\rangle$.

For magnetic coupling of two fragments with total spins of $S_1$ and $S_2$, the resulting state may possess a total spin $S_{\mathrm{t}}$ = $S_1-S_2, S_1-S_2+1,\cdots, S_1+S_2,(S_1>S_2)$ according the well-established rule of angular momentum addition. As elaborated above, the spin wavefunction, $|S,M\rangle$, of a system involving metal-ligand magnetic coupling could be built up by the spin eigenfunctions of two constituent fragments, $|S_1,M_1\rangle$ and $|S_2,M_2\rangle$. Of note, as required by the symmetry of CGCs, $M$= $M_1+M_2$. Geometrically, this means that the z component of the vector sum of two angular momenta is equal to the algebraic sum of their z components. For ferromagnetic coupling with $S_{\mathrm{t}}$ = $S_1+S_2$, the spin eigenfunction,$|S_1+S_2,S_1+S_2\rangle$, of its standard component could also be represented by a single Slater determinant constructed by combination of two single Slater determinants distinguished by $|S_1,S_1\rangle$ and $|S_2,S_2\rangle$ for the two constituent fragments into one. Thus, such systems can be properly treated with DFT, for instance, the septet reaction of $O_2$ with Fe(II)(BDPP). As demonstrated in **Fig. 5**, the spin populations on Fe center and $O_2$ ligand estimated by B3LYP computations for $^7$**A** (3.62 for Fe(II) and 1.99 for $O_2$) and $^7$**1** (4.10 for Fe(III) and 1.20 for $O_2^{\cdot-}$) are all in line with those (3.86 for Fe(II) and 2.00 for $O_2$ in $^7$**A**, 4.74 for Fe(III) and 1.03 for $O_2^{\cdot-}$ in $^7$**1**) derived from CASSCF(12,9) calculations. Moreover, the computed $\hat{S}^2$ expectation values of $\langle\hat{S}^2\rangle$ = 12.00 for $^7$**A** and $\langle\hat{S}^2\rangle$ = 12.00 for $^7$**1** indicate that both B3LYP solutions are devoid of considerable spin contamination and are eigenfunctions of $\hat{S}^2$ having well-defined energies.

The situation is distinctly different for antiferromagnetic coupling where the resulting state has a total spin of $S_{\mathrm{t}}$ < $S_1+S_2$, the wavefunction of its standard component, $|S_{\mathrm{t}},S_{\mathrm{t}}\rangle$, cannot be represented as a single determinant, but has to be constructed as a linear combination of a range of Slater determinants with the eigenvalue of $\hat{S}_z$ of $S_{\mathrm{t}}$ to fulfill the requirement of spin symmetry. Therefore, in principle, DFT cannot be used to computed electronic structures of such systems.

For one particular case with $S_{\mathrm{t}}$ = $S_1-S_2$, its standard component $|S_1-S_2,S_1-S_2\rangle$ again should be built up as a linear combination of $|S_1,S_1|S_2,-S_2\rangle$, $|S_1,S_1-1|S_2,-S_2+1\rangle$, ⋯ , all featuring the same the $\hat{S}_z$ eigenvalue of $S_1-S_2$. Importantly, the first one could be described as a single Slater determinant through combination of two single Slater determinant characterized by $|S_1,S_1\rangle$ and $|S_2,-S_2\rangle$ for the two constituent fragments into one. Broken symmetry formalism exploits this feature, and approximate $|S_1-S_2,S_1-S_2\rangle$ as $|S_1,S_1|S_2,-S_2\rangle$, which means just choosing the first component from the above series. Consequently, the resulting solution is no longer the eigenfunction of $\hat{S}^2$ and spin density and spin populations derived from broken symmetry calculations are not correct. Generally speaking, large spin contamination should be regarded as a characteristics of broken symmetry solutions that can be used to differentiate it from usual “spin-pure” solution discussed above. A case in point is complex $^2$**C** where spin populations of 2.59 for Co(II) and -1.99 for $O_2$ provided by broken symmetry B3LYP calculations are in line with the expected values for $\left|\frac{3}{2},\frac{3}{2}\right|1,-1\rangle$ (**Fig. 5**). These erroneous values that are far from those (1.58 for Co(II) and -0.66 for $O_2$) derived from CASCSF(13,9) calculations nevertheless indicate that the local spins of the Co(II) center and the $O_2$ ligand are $\frac{3}{2}$ and 1, respectively, thus yielding a correct bonding description of complex $^2$**C**. However, this DFT solution suffers from unacceptable spin contamination with $\langle\hat{S}^2\rangle$ = 2.77. As a consequence, its energy is not reliable, because it is not the eigenfunction of the Hamiltonian operator, $\hat{H}$, either. As shown in **Fig. 5**, complex $^5$**1** also belongs to this category.

While for other resulting state of $S_\mathrm{t}$ where $S_1$-$S_2$ < $S_\mathrm{t}$ < $S_1$+$S_2$, its standard component cannot be approximately by a single Slater determinant any more. For example, $S_\mathrm{t} = S_1 + S_2 - 1$, its standard component characterized by $|S_1 + S_2 - 1, S_1 + S_2 - 1\rangle$ should be constructed as a linear combination of the wavefunction distinguished by $|S_1,S_1 - 1|S_2,S_2\rangle$ and $|S_1,S_1|S_2,S_2 - 1\rangle$. As elaborated above, both $|S_1,S_1 - 1\rangle$ and $|S_2,S_2 - 1\rangle$ cannot be represented by a single Slater determinant; hence, neither can $|S_1,S_1 - 1|S_2,S_2\rangle$ nor $|S_1,S_1|S_2,S_2 - 1\rangle$. Thus, DFT completely fails for this kind of system as exemplified by complex $^5$**A**. As depicted in **Fig. 5**, spin populations on Fe(II) of 1.90 and $O_2$ of 1.99 for $O_2$ erroneously predicted by DFT calculations indicate that the converged B3LYP solution with $\langle\hat{S}^2\rangle$ = 6.55 is best interpreted as a triplet Fe(II) center ($S_\mathrm{Fe}$ = 1) ferromagnetically coupled to a triplet $O_2$ ligand ($S_{O_2}$ = 1); therefore, the local spins of Fe and $O_2$ are qualitatively wrong.

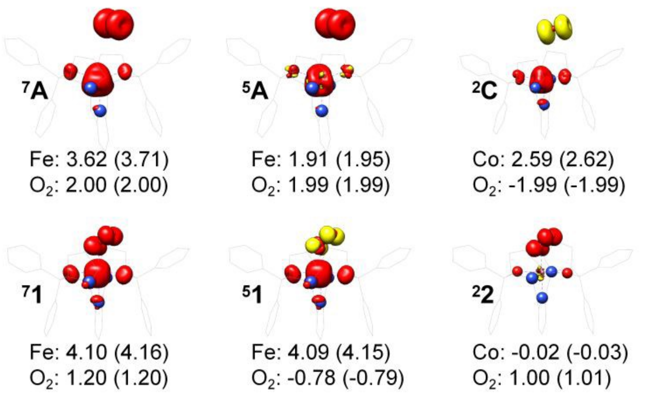

**Fig. 5** Spin density and Löwdin and Mulliken (in parentheses) spin populations for meter center and the $O_2$ ligand from DFT calculations; ligand atoms are omitted for clarity.

In summary, only systems possessing two ferromagnetically coupled fragments, DFT calculations can be used to compute their electronic structures and spin density and spin populations and give reliable energies; otherwise, DFT computations in principle produce incorrect electronic structures and spin density and spin populations. For states with $S_\mathrm{t} = S_1 - S_2$, the electronic structure can be approximately computed by invoking broken symmetry formalism in the framework of DFT calculations. But interpreting the resulting spin density and populations need particular caution. In particular, for open-shell singlets the artificial spin density delivered by broken symmetry calculations is qualitatively incorrect, because there does not exist any spin density everywhere for diamagnetic systems irrespective of being closed-shell or open-shell singlets. For comparison, DFT computed potential energy surfaces are summarized in the Supporting Information.

## Conclusions

CASSCF/NEVPT2 calculations were employed to explore the electronic-structure evolution over the course of $O_2$ binding on Co(II) and Fe(II) precursors affording Fe(III)-$O_2^{-\cdot}$(**1**) and Co(III)-$O_2^{-\cdot}$(**2**) complexes. For the former reaction on the septet and quintet potential surfaces, starting complex $^{7,5}$**A** is best formulated as a high spin Fe(II) center ($S_\mathrm{Fe}$ = 2) ferromagnetically or magnetically coupled with a triplet $O_2$ ligand ($S_{O_2}$ = 1), while product $^{7,5}$**1** consists of a high spin Fe(III) center ($S_\mathrm{Fe}$ = $\frac{5}{2}$) ferromagnetically or antiferromagnetically coupled a superoxo ligand ($S_{O_2^{-\cdot}}$ = $\frac{1}{2}$). Regarding the latter reaction in an $S = \frac{1}{2}$ state, initial complex $^2$**C** could be best characterized as a high spin Co(II) center ($S_\mathrm{Co}$ = $\frac{3}{2}$) antiferromagnetically coupled to a triplet $O_2$ ligand ($S_{O_2}$ = 1). While $O_2$ adduct $^2$**2** contains a low spin Co(III) center ($S_\mathrm{Co}$ = 0) interacting with a superoxo ligand ($S_{O_2^{-\cdot}}$ = $\frac{1}{2}$). As $O_2$ steadily approaches the divalent metal center, the diabatic energy curve of M(II)-$O_2$ constantly rises in energy and interacts with that of M(III)-$O_2^{-\cdot}$ at the M-$O_2$ distance around ~2.40 Å. This interaction generates an avoided crossing that effects a spontaneous single-electron transfer from the divalent metal center to the incoming $O_2$ ligand, thereby leading to M(III)-$O_2^{-\cdot}$ as the final product and ruling out the possibility of formation of an bona fide M(II)-$O_2$. This view has been used to explain reaction outcomes of related $O_2$ association processes.

To extract electronic-structure information from complicated multireference wavefunctions, we constructed two-fragment spin eigenfunctions with CGCs to rationalize computed spin density and fragment spin populations on metal centers and $O_2$ moieties and deduced corrected electronic-structure formulations. This approach is complementary to usual VB analyses as demonstrated by applications of both methods to analyze the electronic-structure of $O_2$ adduct $^5$**1**. This species features antiferromagnetic coupling of a high spin Fe(III) center ($S_\mathrm{Fe}$ = $\frac{5}{2}$) and a superoxo ligand ($S_{O_2^{-\cdot}}$ = $\frac{1}{2}$); however, directly reading out electron configurations of the resulting authenticated multireference wavefunctions hardly gains any chemically sensible bonding information.

For antiferromagnetically coupled systems with $S_\mathrm{t} = S_1 - S_2$, DFT calculations, despite giving a right electronic structure, invariably come at the price of spin contamination, and completely fails for systems with $S_\mathrm{t} < S_1 - S_2$ in predicting qualitatively correct electronic structures. Only for ferromagnetically coupled systems with $S_\mathrm{t} = S_1 + S_2$, DFT is able to give exact electronic structures and energies.

## Author Contributions

S. Y. conceived the presented idea. P. Z. performed the computations and wrote the original draft. S. Y. and W. L. reviewed and edited the final draft. All authors discussed the results and contributed to the final manuscript.

## Conflicts of interest

There are no conflicts to declare

## Acknowledgements

The work in Dalian was supported by National Key R&D Program of China (No. 2021YFA1502803), the National Natural Science Foundation of China (92161204) and Dalian Institute of Chemical Physics, Chinese Academy of Sciences (Grant: DICP I202312). W. L. is grateful for the financial support from the Ministry of Science and Technology of Taiwan (MOST 111-2113-M-003-008-MY3 to W.-Z.L.). We are indebted to Mr. Haowei Chen for helpful discussions.

Notes and references

View Article Online
DOI: 10.1039/D4CP02915A

1 M. Costas, M. P. Mehn, M. P. Jensen and L. Que Jr, *Chem. Rev.*, 2004, **104**, 939.
2 E. G. Kovaleva and J. D. Lipscomb, *Nat. Chem. Biol.*, 2008, **4**, 186.
3 E. I. Solomon, D. E. Heppner, E. M. Johnston, J. W. Ginsbach, J. Cirera, M. Qayyum, M. T. Kieber-Emmons, C. H. Kjaergaard, R. G. Hadt, and L. Tian, *Chem. Rev.*, 2014, **114**, 3659.
4 C. E. Elwell, N. L. Gagnon, B. D. Neisen, D. Dhar, A. D. Spaeth, G. M. Yee and W. B. Tolman, *Chem. Rev.*, 2017, **117**, 2059.
5 X. Huang and J. T. Groves, *Chem. Rev.*, 2017, **118**, 2491.
6 A. J. Jasniewski and L. Que, Jr., *Chem. Rev.*, 2018, **118**, 2554.
7 L. Pauling, C. D. Coryell, *Proc. Natl. Acad. Sci. USA*, 1936, **22**, 210.
8 B. A. Springer, S. G. Sligar, J. S. Olson, and G. N. Jr. Phillips, *Chem. Rev.*, 1994, **94**, 699.
9 K. Shikama, *Chem. Rev.*, 1998, **98**, 1357.
10 J. E. Baldwin, M. Bradley, *Chem. Rev.*, 1990, **90**, 1079.
11 P. L. Roach, I. J. Clifton, V. Fülöp, K. Harlos, G. J. Barton, J. Hajdu, I. Andersson, C. J. Schofield, J. E. Baldwin, *Nature*, 1995, **375**, 700.
12 P. L. Roach, I. J. Clifton, C. M. H. Hensgens, N. Shibata, C. J. Schofield, J. Hajdu, J. E. Baldwin, *Nature*, 1997, **387**, 827.
13 J. H. Jeoung, M. Bommer, T.-Y. Lin, H. Dobbek, *Proc. Natl. Acad. Sci. USA*., 2013, **110**, 12625.
14 G. J. Christian, F. Neese, S. Ye, *Inorg. Chem*., 2016, **55**, 3853.
15 G. J. Christian, S. Ye, F. Neese, *Chem. Sci*., 2012, **3**, 1600.
16 L. Que Jr., and R. Y. N. Ho, *Chem. Rev*., 1996, **96**, 2607.
17 E. I. Solomon, T. C. Brunold, M. I. Davis, J. N. Kemsley, S. Lee, N. Lehnert, F. Neese, A. J. Skulan, Y. Yang, and J. Zhou, *Chem. Rev*., 2000, **100**, 235.
18 R. A. Baglia, J. P. T. Zaragoza, and D. P. Goldberg, *Chem. Rev*., 2017, **117**, 13320.
19 S. Yadav, V. Yadav, M. A. Siegler, P. Moënne-Loccoz, G. N. L. Jameson, D. P. Goldberg, *J. Am. Chem. Soc.*, 2024, **146**, 12, 7915.
20 C. Winslow, H. Lee, M. J. Field, S. J. Teat, J. Rittle, *J. Am. Chem. Soc.*, 2021, **143**, 34, 13686.
21 M. N. Blakely, M. A. Dedushko, P. C. Y. Poon, G. Villar-Acevedo, J. A. Kovacs, *J. Am. Chem. Soc.*, 2019, **141**, 5, 1867.
22 J. Sacramento, T Albert, M Siegler, P Moënne-Loccoz, D. P. Goldberg, *Angew. Chem. Int. Ed*. **2022**, 61, e202111492.
23 C. Chiang, S. T. Kleespies, H. D. Stout, K. K. Meier, P. Li, E. L. Bominaar, L. Que Jr., E. Münck and W. Lee, *J. Am. Chem. Soc.*, 2014, **136**, 10846.
24 P. Zhang, Y. Tian, Z. Wang, W. Lee, and S. Ye, *Chem. Eur. J.* 2024, **30**, e202400336
25 C. Wang, H. Chang, Y. Lai, H. Fang, C. Li, H.Hsu, Z. Li, T. Lin, T. Kuo, F. Neese, S. Ye, Y. Chiang, M. Tsai, W. Liaw, and W. Lee, *J. Am. Chem. Soc.*, 2016, **138**, 14186.
26 A. J. Fielding, J. D. Lipscomb, L. Que Jr., *J. Am. Chem. Soc.*, 2012, **134**, 796.
27 F. A. Walker and J. Bowen, *J. Am. Chem. Soc.*, 1985, **107**, 7632.
28 J. B. Gordon, A. C. Vilbert, M. A. Siegler, K. M. Lancaster, P. Moënne-Loccoz, D. P. Goldberg, *J. Am. Chem. Soc.*, 2019, **141**, 5, 3641.
29 P. Kumar, S. V. Lindeman, A. T. Fiedler, *J. Am. Chem. Soc.*, 2019, **141**, 10984.
30 A. Huber, L. Müller, H. Elias, R. Klement, M. Valko, *Eur. J. Inorg. Chem*. 2005, 1459.
31 J. Yang, P. Li, X. Li, L. Xie, N. Wang, H. Lei, C. Zhang, W. Zhang, Y.-M. Lee, W. Zhang, R. Cao, S. Fukuzumi, W. Nam, *Angew. Chem. Int. Ed*. 2022, **61**, e202208143.
32 Y. Lin, H. Hinrika Cramer, M. van Gastel, Y. Tsai, C. Chu,T. Kuo, I. Lee, S. Ye, E. Bill, and W. Lee, *Inorg. Chem*. 2019, **58**, 9756.
33 H. Pan, H. Chen, Z. Wu, P. Ge, S. Ye, G. Lee, and H. Hsu, *JACS Au*, 2021, **1**, 1389.
34 E. G. Kovaleva, M. B. Neibergall, S. Chakrabarty, and J. D. Lipscomb, *Acc. Chem. Res.*, 2007, **40**, 475.
35 S. M. Adam, G. B. Wijeratne, P. J. Rogler, D. E. Diaz, D. A. Quist, J. J. Liu, and K. D. Karlin, *Chem. Rev.*, 2018, **118**, 10840.
36 E. G. Kovaleva and J. D. Lipscomb, *Science*, 2007, **316**, 453.201
37 M. M. Mbughuni, M. Chakrabarti, J. A. Hayden, E. L. Bominaar, M. P. Hendrich, E. Münck, and J. D. Lipscomb, *Proc. Natl. Acad. Sci. USA*, 2010, **107**, 16788.
38 M. M. Mbughuni, K. K. Meier, E. Munck, and J. D. Lipscomb, *Biochemistry*, 2012, **51**, 8743.
39 M. Radon and K. Pierloot, *J. Phys. Chem. A*, 2008, **112**, 11824.
40 H. Chen, M. Ikeda-Saito, and S. Shaik, *J. Am. Chem. Soc.*, 2008, **130**, 14778.
41 S. Shaik and H. Chen, *J. Biol. Inorg. Chem*., 2011, **16**, 841.
42 H. Chen, K. Cho, W. Lai, W. Nam, and S. Shaik, *J. Chem. Theory Comput*., 2012, **8**, 915.
43 G. J. Christian, S. Ye, and F. Neese, *Chem. Sci.*, 2012, **3**, 1600.
44 S. Ye, C. Riplinger, A. Hansen, C. Krebs, J. M. Bollinger, Jr., and F. Neese, *Chem. Eur. J.*, 2012, **18**, 6555.
45 K. P. Jensen, B. O. Roos, and U. Ryde, *J. Inorg. Biochemistry*, 2005, 99, 45.
46 K. P. Kepp, *ChemPhysChem*, 2013, **14**, 3551.
47 Q. M. Phung and K. Pierloot, *Phys. Chem. Chem. Phys.*, 2018, **20**, 17009.
48 L. Noodleman, *J. Chem. Phys*., 1981, **74**, 5737.
49 J. Ribas-Arino, and J. J. Novoa, *Chem. Commun.*, 2007, 3160.
50 P. Malmqvist, B. O. Roos, *Chem. Phys. Lett*., 1989, **155**, 189.
51 C. Angeli, R. Cimiraglia, J.-P. Malrieu, *J. Chem. Phys*., 2002, **117**, 9138.
52 C. Angeli, R. Cimiraglia, S. Evangelisti, T. Leininger, J. P. Malrieu, *J. Chem. Phys.*, 2001, **114**, 10252.
53 M. E. Rose, Elementary theory of angular momentum, Dover Publications Inc., New York, 1957.
54 A. D. Becke, *J. Chem. Phys*., 1993, **98**, 5648.
55 C. Lee, W. Yang, R. G. Parr, *Phys. Rev. B*, 1988, **37**, 785.
56 A. D. Becke, *Phys. Rev. A*, 1988, **38**, 3098.
57 A. Schäfer, C. Huber, R. Ahlrichs, *J. Chem. Phys*., 1994, **100**, 5829.
58 J. P. Perdew, K. Burke, M. Ernzerhof, *Phys. Rev. Lett*., 1996, **77**, 3865.
59 F. Weigend, R. Ahlrichs, *Phys. Chem. Chem. Phys*., 2005, **7**, 3297.
60 A. Schäfer, H. Horn, R. Ahlrichs, *J. Chem. Phys*., 1992, **97**, 2571
61 S. Kossmann, F. Neese, *J. Chem. Theory Comput.*, 2010, **6**, 2325.
62 K. Eichkorn, O. Treutler, H. Öhm, M. Häser, R. Ahlrichs, *Chem. Phys. Lett*., 1995, **242**, 652.
63 F. Weigend, *Phys. Chem. Chem. Phys*., 2006, **8**, 1057.
64 V. Barone, M. Cossi, *J. Phys. Chem. A, 1998*, **102**, 1995.
65 S. Grimme, S. Ehrlich, L. Goerigk, *J. Comput. Chem*., 2011, **32**, 1456.
66 S. Grimme, J. Antony, S. Ehrlich, H. Krieg, *J. Chem. Phys.*, 2010, **132**, 154104
67 C. Kollmar, K. Sivalingam, B. Helmich-Paris, C. Angeli, F. Neese, *J. Comput. Chem*., 2019, **40**, 1463.
68 F. Weigend, *J. Comput. Chem*., 2008, **29**, 167.
69 F. Neese, F. Wennmohs, U. Becker, C. Riplinger, *J. Chem. Phys*., 2020, **152**, 224108.
70 H. Chen, M. I.-S., S. Shaik, *J. Am. Chem. Soc.*, 2008, **130**, 14778.
71 D. Maiti, H. C. Fry, J. S. Woertink, M. A. Vance, E. I. Solomon, K. D. Karlin *J. Am. Chem. Soc*. 2007, **129**, 26.
72 C. Wrtele, E. Gaoutchenova, K. Harms, M. C. Holthausen, J. Sundermeyer, S. Schindler, *Angew. Chem. Int. Ed*. 2006, **45**, 3867.
73 S. Y. Quek, S. Debnath, S. Laxmi, M. van Gastel, T. Krämer, J. England, *J. Am. Chem. Soc.*, 2021, **143**, 47, 19731.
74 R. Trammell, K. Rajabimoghadam, I. Garcia-Bosch, *Chem. Rev*., 2019, **119**, 2954
75 C. E. Elwell, N. L. Gagnon, B. D. Neisen, D. Dhar, A. D. Spaeth, G. M. Yee, W. B. Tolman, *Chem. Rev*., 2017, **117**, 2059.
76 S. Fukuzumi, K. D. Karlin, *Coor. Chem. Rev*., 2013, **257**, 187.
77 S. Hong, Y. Lee, K. Ray, W. Nam, *Coor. Chem. Rev*., 2017, **334**, 25.
78 H. Noh, J. Cho, *Coor. Chem. Rev*., 2019, **382**, 126.

View Article Online
DOI: 10.1039/D4CP02915A

The data supporting this article have been included as part of the Supplementary Information.